Attomolar label-free detection of DNA hybridization with electrolyte-gated graphene field-effect transistors

Rui Campos[†,ζ], Jérôme Borme[†], Joana Rafaela Guerreiro[‡], George Machado Jr[†,#], Maria Fátima Cerqueira[†,#], Dmitri Y Petrovykh[‡], and Pedro Alpuim[†,#,*]

[†] Department of Quantum and Energy Materials, INL – International Iberian Nanotechnology Laboratory, 4715-330, Braga, Portugal

[‡] Department of Life Sciences, INL – International Iberian Nanotechnology Laboratory, 4715-330, Braga, Portugal

[#]CFUM – Center of Physics, University of Minho, 4710-057, Braga, Portugal

KEYWORDS: Biosensor, graphene, DNA, EGFET (electrolyte-gated field-effect transistor), planar technology, receded gate transistor, surface functionalization

ABSTRACT: In this work, we develop a field-effect transistor with a two-dimensional channel made of a single graphene layer to achieve label-free detection of DNA hybridization down to attomolar concentration, while being able to discriminate a single nucleotide polymorphism (SNP). The SNP-level target specificity is achieved by immobilization of probe DNA on the graphene surface through a pyrene-derivative heterobifunctional linker. Biorecognition events result in a positive gate voltage shift of the graphene charge neutrality point. The graphene transistor biosensor displays a sensitivity of 24 mV/dec with a detection limit of 25 aM: the lowest target DNA concentration for which the sensor can discriminate between a perfect-match target sequence and SNP-containing one.

DNA detection platforms are developing at a dizzying pace as they provide information to a wide range of fields, including, molecular biology research,[1] genetic disease diagnosis,[2] biological informatics,[3] forensics[4] and environmental monitoring[5]. Field-effect transistors are an alternative to the common methods for the detection of DNA (polymerase chain reaction (PCR)[6] and optical[7] and electrochemical techniques[7,8]) with the advantage of allowing for high sensitivity, specificity and short measurement time without the need of labelling. Moreover, field-effect transistor (FET) technology lends itself to microfabrication at the wafer scale and, due to the small footprint of the devices, a large number can be placed in a single chip. Biosensors based on FETs (bio-FETs) are functionalized with a biological recognition element that captures the target molecule, producing an electrostatic gating effect.[9]

The transistor channel in a standard FET, *e.g.*, in the metal-oxide-semiconductor FET (MOSFET), forms at the interface between a bulk semiconductor, *e.g.*, silicon, and a dielectric thin film, e.g., silicon oxide.[10] The semiconductor-dielectric interface is buried inside the device, therefore not accessible for functionalization. Consequently, the surfaces for biorecognition are, either an extension of the gate contact (like in charge-modulated FETs), or the surface of the gate oxide itself (like in ion-sensitive ISFETs).[11] These surfaces are then exposed to the medium carrying the analyte and, whenever biorecognition events occur, they modulate the gate capacitance, and therefore the electric field across the gate dielectric resulting from the applied gate voltage. The gate dielectric must be thin, to lower the operating voltage and increase the transconductance, which dictates the device sensitivity, but cannot be so thin as to increase the leakage current beyond acceptable levels, or cause electric disruption of the dielectric material. These restrictions limit the sensitivity of bio-FETs based on conventional FET architectures.

Almost all of the above challenges can be addressed more efficiently by a graphene electrolyte-gated FET (EGFET).[12] Because the transistor channel is formed by a one-atom-thick graphene layer, at least one of its surfaces can be left accessible for functionalization. The local gating effect is much more effective than in conventional devices, because now the charged species modulating the electric field can be directly attached to the transistor channel. And the electrical double layers (EDLs) that form at the graphene-electrolyte and electrolyte-gate contact interfaces, with characteristic thickness given by the Debye length (d_D) (just a few tens of Angstroms thick), replace the solid gate dielectric. The resulting EDL capacitance is huge and allows operating the device at very low gate voltage (V_{GS}), with very high transconductance. Moreover, V_{GS} can be applied in a receded contact, placed far away from the transistor channel, across a vast volume of solution (as compared with the volume defined by the d_D), because the V_{GS} drops essentially in the EDLs.[11,13]

One-dimensional materials, e.g., carbon nanotubes and silicon nanowires, can also be used in high-sensitivity EGFETs[14,15] based on the same working principles, and with similar advantages, but due to the difficulty and cost of large-scale fabrication their use is limited.[9] Besides, control of structural and electronic properties of 1D materials is, so far, elusive, resulting in a large variability in device performance.[16] Two-dimensional materials, compatible with standard planar technology, present themselves as logical alternatives for bio-FET development, with graphene leading the way[15,17,18] for other promising materials.[16,19]

FETs made of single layer graphene (SLG) present better detection limits than those made of graphene oxide or few-layer graphene,[20–22] mainly because they have a much higher transconductance. Zheng *et al.*[23] showed an improvement, from 100 fM to 10 fM, in the detection limit of PNA/DNA hybridization, when they changed from rGO to chemical vapor deposited (CVD) monolayer graphene.[23,24] Moving from single graphene FETs to an array composed of six CVD graphene FETs, Xu *et al.*[25] detected DNA hybridization down to 100 fM. Either through direct adsorption of the oligonucleotide on the graphene surface[20,22] or through the use of linkers,[23–27] the reported DNA hybridization detection limits are in the fM range.

EGFETs essentially sense phenomena that occur inside a volume set by the width of the Debye layer. Changing the ionic strength of the buffer, therefore, implies a change in the volume of detection of hybridization events. Higher ionic strength promotes hybridization, since it screens more of the negative charge of the DNA backbone, but lower ionic strength is equivalent to an expanded EDL, with an increased space-charge volume for sensing, and consequently an expanded range of detection of the hybridization process.[25,27] With this in mind Chen *et al.*[21] used a low-ionic-strength buffer and showed an improvement to the detection limit in the pM range.

Here, we develop a CVD-grown SLG receded-gate field-effect transistor for label-free detection of target DNA with high specificity and ultra-high sensitivity. The specificity is intrinsic to DNA biorecognition when using a DNA probe perfectly matched to the DNA target, while the sensitivity comes from the transducing capability of the graphene-electrolyte interface of the EGFET. The transistor performance is enhanced by its architecture, with a large-area in-plane gate surrounding the graphene channel placed at its centre (gate area is ≈ 2500 times larger than channel area), providing a uniform distribution of the potential inside the water droplet and a very uniform gating field. The large overlapping between graphene and gold over the source and drain contacts (overlapping area in each contact is ≈ 2.35 larger than channel area), provides ohmic contacts. In this way, DNA hybridization is detected down to 25 aM while maintaining the ability to detect single nucleotide polymorphism (SNP) in the DNA target strand.

MATERIALS AND METHODS

Materials. All components of buffer solutions (Na_2HPO_4, NaH_2PO_4, NaCl, $MgCl_2$, 1-Dodecanethiol (DDT) and 1 – pyrenebutyric acid succinimidyl ester (PBSE) and all the solvents were from Sigma–Aldrich. Ultrapure water (18 MΩ cm, Millipore, Bedford, MA, USA) was used throughout the experiments. The probe DNA (pDNA), with a 3' C7-amino modification (5'- TCA TAA CCG GCG AAA GGC TGA AGC T-3'), the complementary DNA (5'-AGC TTC AGC CTT TCG CCG GTT ATG A-3'), the SNP containing target (5'-AGC TTC AGC CTT <u>A</u>CG CCG GTT ATG A-3') and the probe complimentary to the SNP sequence with a 3' C7-amino modification (5'- TCA TAA CCG GCG TAA GGC TGA AGC T-3') were synthesized by Metabion International AG, Martinsried, Germany. The melting temperature, T_m, of the DNA duplex was estimated using DINAMelt web server[28], and was 82.7 °C (80.4 °C for SNP containing duplex and 82.3 °C for the fully complimentary SNP) in the hybridization buffer (10 mM PB/150 mM NaCl/50 mM $MgCl_2$) and 58.9 °C (54.8 °C for SNP containing duplex and 58.5 °C for the fully complimentary SNP) in the working buffer solution (10 mM PB).

High purity (> 99.99 %) coper foil for graphene growth was purchased from Alfa-Aesar or Goodfellow.

EGFET Fabrication. A detailed procedure is described elsewhere[29,30] and briefly given here. The fabrication of the contacts is performed on 200 mm Si (100) wafer (B-doped, 8-30 Ω, LG Siltron) with 200 nm of thermal oxide. A sputtered layer of Cr 3 / Au 30 nm is used as the contact material. The source, drain and gate contacts are patterned using optical lithography (channel size 25 μm × 75 μm) then etched by ion milling. A 250 nm multilayer of silicon nitride and silicon oxide is grown by chemical vapor deposition. An optical lithography defines the area of the current lines to be protected by the passivation. Reactive ion etching is used to remove the passivation from outside the current lines. The drain, source and gate contacts were previously covered with a layer containing aluminium, which stops the reactive ion etch. After etching, the stopping layer is removed by wet etch. A thin aluminium oxide layer (10 nm) is deposited uniformly, and patterned by optical lithography and wet etching to open the channel, source and drain contacts. Graphene is then transferred. An optical lithography protects the area of the source, drain and channel. An oxygen plasma is used to pattern graphene. The aluminium oxide layer is removed using wet etch. The wafer is then coated with photoresist as a protection and diced into individual dies.

Graphene growth and transfer. Single-layer graphene is grown by thermal chemical vapour deposition on high purity copper foils. The copper foil is cut into 10 cm × 10 cm parts and fit into a graphite confinement box which isolates the substrate from sources of contamination. The substrate is introduced into a three zone quartz tube furnace (EasyTube ET3000, CVD Corp.) and first annealed at 1020 °C for 20 min in hydrogen atmosphere (300 sccm, 0.5 torr). The gaseous carbon source is a mixture of methane

and hydrogen (H_2:CH_4 6:1, 0.5 torr) that flows into the furnace for 30 min, while keeping the temperature at 1020 °C. After growth, graphene is transferred by a standard procedure using a PMMA temporary substrate (see SI).

Transistor architecture. The transistor architecture is planar, with a receded gate.[30] The source and drain are two semi-circular contacts of 75 µm of diameter, separated by a 25 µm gap which constitutes the graphene channel (see Figure 1). A concentric 2-lobe annular gate is placed at 50 µm distance from source and drain. The total gate diameter is 3 mm and presents an area that is 2480 times larger than the channel area.

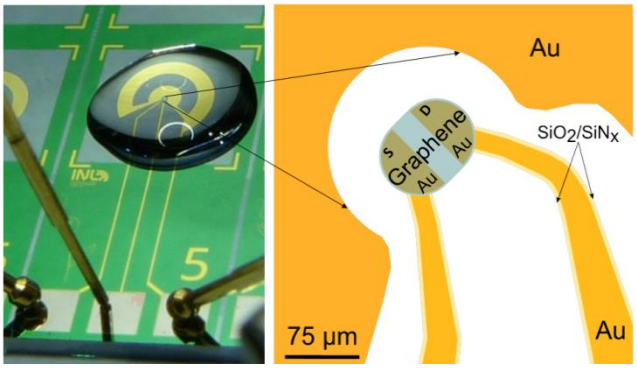

Figure 1. (left) Optical image of one transistor chip under measurement; (right) drawing of the transistor zoomed-in channel region, showing source (S), drain (D), gate (partial view), channel, and Au contact lines with SiO2/SiNx passivation layer.

EGFET functionalization with DNA. The fabricated chips, protected with photoresist for the dicing, were washed with acetone and then immersed in ethyl acetate for 2 hours. The development of the DNA biosensor is schematically illustrated in Figure S1 of the SI. The Au receded gate is passivated with DDT[31] (overnight, 2 mM ethanol solution) to avoid adsorption of DNA on the Au surface (stage 1). Au source and drain contact areas that may be exposed due to discontinuities in the graphene layer covering them, are also passivated in this stage. In stage 2, the graphene surface is functionalized with PBSE[32] (immersion in 10 µL of a 10 mM solution in dimethylformamide (DMF), for 2 hours, followed by rinsing with DMF, H_2O and drying with N_2). The PBSE molecule contains a pyrene group that binds to graphene via π-π interaction, and an ester group at the other end, which reacts with primary amines. Probe DNA is immobilized by NHS reaction by placing a 10 µL drop of 10 µM pDNA in buffer (overnight, in wet chamber at 4 °C) on the graphene surface modified with PBSE. The last step (stage 4) before target DNA detection (stage 5) is the passivation of the graphene surface with ethanolamine (10 µL of 100 mM solution in 10 mM PB, pH 8.5, 30 minutes[33]) which reacts with the molecules of PBSE that did not react with the DNA probes.

RESULTS AND DISCUSSION

The EGFETs used here were fabricated at the 200-mm wafer scale, with multiple chips in each wafer. An optical image of an EGFET is shown in Figure 1, with the source, drain and gate contacts clearly visible. The transistor channel is at the center of the surrounding two-lobbed annular gate, providing a uniform distribution of the electric potential in the vicinity of the channel. The large overlap area between graphene and Au over the entire source and drain surface makes good ohmic contacts to the channel. Graphene coverage of the source and drain Au contacts, prevents the Au surfaces from exposure to the solutions and biomolecules contained therein, which renders the measurements more reliable. After fabrication, the wafer is diced into individual chips that are used for the biosensor development.

DNA biosensor development.

Transfer curves, TCs, *i.e.* records of the drain-source current, I_{DS}, under constant drain-source voltage, V_{DS}, as a function of the gate-source voltage, V_{GS}, were acquired after each stage of the biosensor development process (top lines in Figure 2 and Figure S2, SI). Raman spectra were acquired after stages 0 (as-fabricated), 1, 2 and 5 (see Materials and Methods and Figure S1 in the SI, where these steps are schematically illustrated). All the TCs were measured in 10 mM phosphate buffer (PB), and, in stage 0, also in ultrapure water (resistivity of 18 MΩ cm), while Raman spectra were acquired on dried samples. Concerning the TC measurements, most devices presented some drift in their TCs when measured repeatedly (Figures S2 and S3, SI), especially during the first few repetitions. Therefore each measurement was repeated 10 times and the data presented in the following sections correspond to the tenth curve acquired in each series of measurements. Each measurement was repeated on five different sensors; hence the results shown are an average of five independent measurements. The complete set of TCs for all the stages and different concentrations can be found in Figure S2, SI.

At stage 0, the TC (Figure 2, black line) shows the typical ambipolar characteristic of a graphene FET. The curve is symmetric around a point of minimum I_{DS}, occurring at a gate voltage V_{Dirac}, where the channel conductivity is at its lowest—corresponding to an electron chemical potential (Fermi level) as close as it can be practically realized to the Dirac point.[34] The steep branches in the curve, to the left and right of V_{Dirac}, correspond to transport by holes and electrons, respectively. The position of V_{Dirac}, shifted to positive values of gate voltage, shows that our graphene is p-doped. This unintentional doping likely originates from residues of process chemicals and is common in CVD-graphene processed by wet transfer.[35]

Nucleic acids adsorb easily onto gold surfaces,[36,37] so the passivation of the Au gate is an important step for preventing the adsorption of both the probe and target DNA sequences on its surface and producing measurement artifacts. The passivation was done in stage 1 (Figure S1) and the TC measurement after this stage leads to a shift

of -100±40 mV in V_{Dirac} (Figure 2, red curve). The shift results from a change of composition of the gate surface, with the formation of a dense self-assembled monolayer (SAM) that covers the Au contact.[21] This process is accompanied by dipole formation at the interface, induced by charge transfer during chemisorption of S on Au and the combined dipole moments of the alkane chains. For common alkanethiols, like DDT, this dipole moment is oriented from the surface into the solution.[38] Consequently, there is a net positively charged layer inside the solution, bound to the surface of the Au, held at V_{GS} by the power supply, which increases the electric field resulting from the applied gate voltage (V_{GS} > 0). Therefore, gating is enhanced and the TC is shifted towards lower values of V_{GS}, as observed in Figure 2, Stage 1 (DDT).

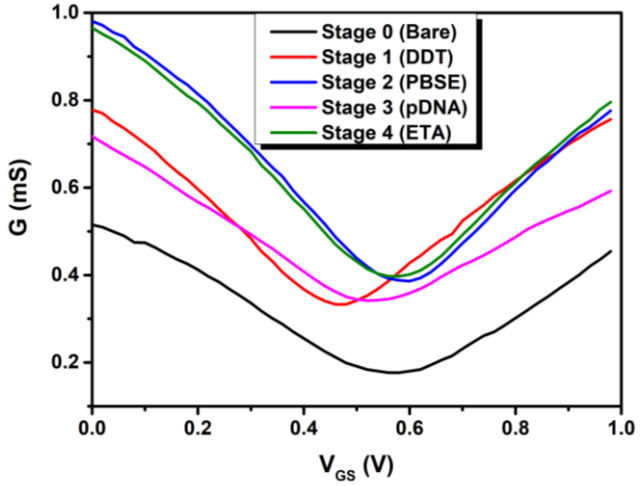

Figure 2. Characteristic transfer curves after each stage of the EGFET channel functionalization.

Stage 2—functionalization of the graphene with PBSE—results in a shift of ΔV_{Dirac} = +40±10 mV (Figure 2, blue line). The functionalization of carbon surfaces with 1-pyrenebutyric acid leads to small shifts in chemical potential, actually smaller than those predicted by molecular dynamics simulations,[39] due to more effective screening by water molecules, which can more readily penetrate between the carboxylic acid group—an ester group in the case of PBSE—and the carbon surface. The large shift observed in the TC after this step (Figure 2, stage 2) is likely due to the surface effects, as confirmed by Raman spectroscopy results (*cf.* Figure S4 and related discussion in the SI). The sign of the TC shift—towards more positive V_{GS}—indicates that there is additional p-doping of the graphene upon π-π stacking of the linker.

The last two functionalization stages are the immobilization of the DNA probes (stage 3) followed by the passivation of the channel with ethanolamine (ETA) (stage 4). Stage 4 is necessary to minimize non-specific reactions. After stage 3, there will be many unreacted NHS-ester ligands that will be blocked by reacting with ETA. After immobilization of the single-stranded DNA (ssDNA) probes via PBSE linkers, there is a large shift of ΔV_{Dirac} ≈ -70 mV between stages 3 and 2. When ETA blocks the unreacted NHS-ester ligands of PBSE, the difference in V_{Dirac} between stages 4 and 2 is reduced to ΔV_{Dirac} ≈ -50 mV. This decrease of ΔV_{Dirac} is likely explained by removal of weakly bound DNA strands from the surface after incubation in the ETA solution (Figure 2, pink and green lines respectively).

The surface density of probe DNA

The density of probe DNA immobilized on the surface of a biosensor will set its dynamic range, and may significantly influence its behaviour.[36,37,40,41] We have used two independent techniques to investigate the surface density of DNA probes achievable on our devices.

Quartz crystal microbalance (QCM) enables *in situ* gravimetric measurements of surface adsorption in solution, with sensitivity sufficient to detect full or partial layers of biomolecules and biorecognition events.[42] With solution parameters adjusted to be compatible with QCM measurements (as described in the SI), we have measured the surface density of DNA probes immobilized on graphene via PBSE to be 1.0±0.1 × 10^{13} cm^{-2}. In all the control experiments, nonspecific adsorption of DNA produced at least 50% lower surface density, in agreement with previous results for DNA immobilization on gold.[37]

X-ray photoelectron spectroscopy (XPS) was used as an *ex situ* technique complementary to QCM, extending the methodology previously developed for quantification of molecular layers on surfaces.[37,43–45] The presence of the NHS-ester ligands of PBSE was confirmed by observing the characteristic[46] N 1s component at 401.6 eV (Figure S5). After DNA immobilization, this NHS-ester N 1s component is replaced by one at 400.8 eV, matching the position expected for the thymine homo-oligonucleotides[37,43] that we used as simulated probes. Furthermore, the N 1s shoulder at ca. 399.3 eV is consistent with a fraction of the probes being in contact with the substrate.[43] The surface density of probes calculated based on the XPS data is 1.5±0.2 × 10^{13} cm^{-2}, in agreement with QCM results and with values previously reported for high-quality DNA-functionalized biosensor surfaces.[36,37,43]

DNA biosensor performance

After the last passivation step (ETA – step 4, Figure S1) the device is ready to detect the target DNA. For each target concentration, a droplet of the solution containing the target was placed on the transistor channel and allowed to interact with the probe DNA for a fixed time interval of 40 min, to allow the hybridization to be accomplished. After this time a stringency rinse using the measuring buffer (10 mM PB, pH 7.4) was performed in order to remove strands that did not hybridize or were weakly bound, and finally the transistor TCs were measured.

Figure 3a shows the EGFET TCs for different concentrations of fully complementary DNA ($cDNA_{PM}$) target. As the concentration of $cDNA_{PM}$ increases, in a range between 1 aM and 100 fM, a progressive shift in V_{Dirac} towards more positive V_{GS} is observed. For [$cDNA_{PM}$] > 100 fM, V_{Dirac} does

not move any more, reaching saturation. The trajectory of V_{Dirac} as a function of [cDNA$_{PM}$] is clearly visible in Figures 4 and S6a where V_{Dirac} is plotted as a function of [cDNA$_{PM}$]. The isoelectric point of DNA is close to 5.0,[47] therefore, at physiological pH, DNA molecules are negatively charged. The electrostatic field of these charges immobilized near the graphene surface will induce, by local gating, *p*-doping, which shifts V_{Dirac} to more positive V_{GS}.[22] Saturation at 100 fM indicates reaching an equilibrium between hybridization and electrostatic repulsion between DNA probes and targets.

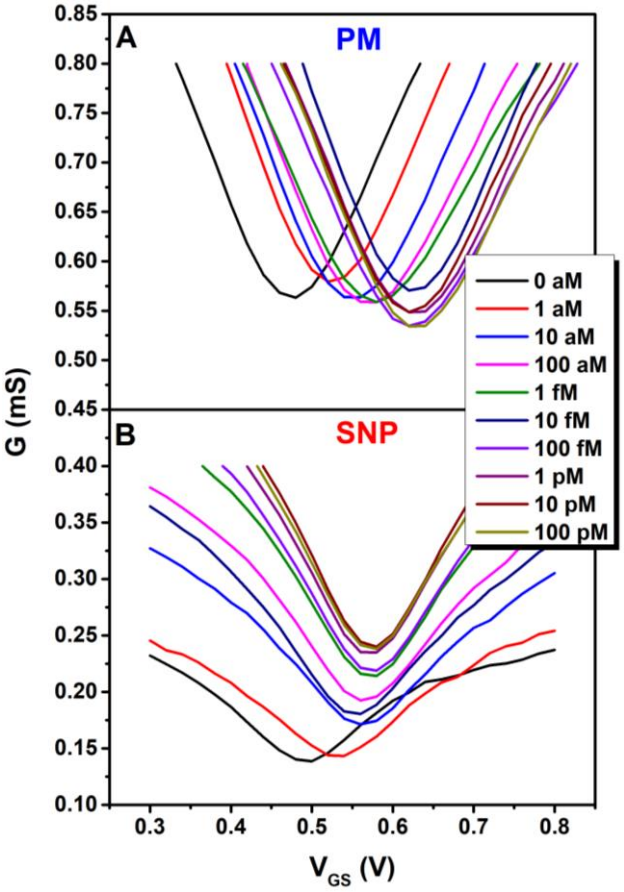

Figure 3. Characteristic transfer curves for: A) Perfect match (PM) complementary DNA, B) SNP containing cDNA, for the different concentrations studied.

In the dynamic range of the biosensor, a sensitivity of 24 mV/decade is achieved, which is an improvement of 7 mV/decade when compared to the best results reported in the literature.[19] In the case of SNP-containing cDNA, the shift of V_{Dirac} with increasing concentrations of cDNA (Figures 3b and 4, red circles) is apparent only as a weak trend, visible upon fitting the entire set of data to a straight line. This behavior is expected since the DNA duplex can still be formed between the probe DNA and the SNP-containing cDNA, but it is unstable and most of the duplexes formed are probably unzipped during the stringency rinse.[23] As a control experiment, a probe DNA fully complementary to SNP-containing target was immobilized on the graphene FET channel and an experiment, conducted in the same manner as before, showed that the sensor could indeed detect the perfectly matching sequence (Figure S6c).

It is important to note that after the probe immobilization in stage 3, ΔV_{Dirac} was negative, whereas upon probe hybridization with target DNA all ΔV_{Dirac} shifts are positive. Table 1 summarizes published data reporting ΔV_{Dirac} shifts observed in liquid-gate bio-FETs based on graphene, or graphene-related materials. With no exception,[20,21,46] upon DNA hybridization, devices that use no linker have $\Delta V_{Dirac} < 0$, while devices using PBSE linkers,[25,47] including ours, have $\Delta V_{Dirac} > 0$. A simple interpretation for the left-shift of V_{Dirac} when no linker is used is duplex DNA desorption from the graphene surface upon probe-target hybridization. This will leave a lower concentration of negatively charged pDNA for local gating on the graphene surface and consequently V_{Dirac} undergoes a negative shift (graphene becomes less *p*-doped). The positive shift upon DNA hybridization observed with PBSE linkers has been discussed above and is a consequence of forming the duplex tethered to the graphene surface via the PBSE linker. These tethered DNA hybrids will not desorb, except for a small fraction of hybrids formed with pDNA directly adsorbed to graphene.

In contrast, the initial immobilization of pDNA on the graphene surface via PBSE has the same effect as that of an electron-donating group ($\Delta V_{Dirac} < 0$). Literature reports on doping single-layer graphene with π-stacked aromatic molecules (e.g., Refs. [49,50]), show that *p*-doping is observed when stacking is with electron-withdrawing groups, and *n*-doping occurs when stacking with electron-donating groups. Because the pDNA single strands are flexible, they can partially interact with the graphene surface via π-π stacking of the nucleobase aromatic rings (pyrimidines and purines), as indicated by the N 1s shoulder at ca. 399.3 eV in XPS data (Figure S5).[43]

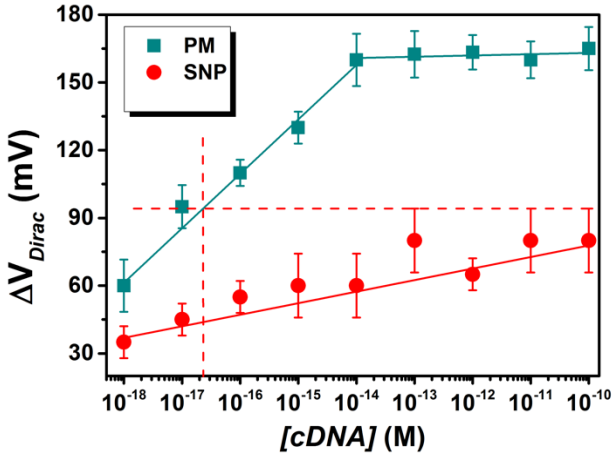

Figure 4. Calibration curves for the bio-FET sensor. Green squares refer to target DNA fully complementary to the probe and red circles to SNP target. The error bars are standard deviations of measurement with 5 different devices.

However, upon DNA hybridization the much stiffer duplex DNA attached covalently to the PBSE linker, will extend away from the surface, overcoming the π-π interaction of

pDNA with the surface. The mechanism of interaction of these upright hybrids with graphene is now exclusively by local gating via modulation of the EDL capacitance, as discussed above.

Table 1. Literature survey of graphene-based electrolyte gated FET DNA biosensor characteristics.

Work	*Limit of Detection[a] (M)*	*Hybridization conditions*	*FET Channel*		*Linker*	*Gate*	*Shift[b] in V_{Dirac}*	*Fabrication*
			Growth/Transfer	L × W (μm²)				
Chen[21]	1×10^{-12}	1× PBS[c]	CVD on Cu/PMMA	$10^4 \times 10^4$	None	Ag-wire	negative	contacts w/ Ag paste
Dong[20]	1×10^{-11}	PB1[d], pH 7.4	CVD on Ni/PMMA	3000 × 10000	None	Ag-wire	negative	contacts w/ Ag-paint
Xu[25]	1×10^{-11}	0.01× PBS pH 7.8	CVD on Cu/PMMA	45 × 90	PBSE	Pt-wire	positive	μ-fluidic platform, optical litho.
Xu[51]	1×10^{-13}	0.01× PBS pH 7.4	CVD on sapphire/ N/A (direct growth)	43 × 90	PBSE	Ag/AgCl wire	positive	μ-fluidic platform, optical litho.
This work	1×10^{-17}	PB2[e], pH 7	CVD on Cu/PMMA	25 × 75	PBSE	Au-planar, integrated	positive	planar, optical litho., contacts pre-patterned

[a] in synthetic medium; [b] upon DNA hybridization; [c] 137 mM NaCl, 2.7 mM KCl, 4.3 mM Na_2HPO4, 1.47 mM KH_2PO4; [d] 10 mM PB, 250 mM NaCl; [e] 10 mM PB, 150mM NaCl, 50 mM $MgCl_2$

Figure 4 shows the sensor output data for the two series of measurements, with perfectly matched (squares) and SNP-containing (circles) targets. The sensor exhibits, for the perfectly matched target, a linear range between 1 aM and 10 fM before saturating at 100 fM. We use the maximum signal from the SNP-containing target in Figure 4, to set the limit of detection (LoD) of the sensor to ≈25 aM, as indicated by the dashed lines in Figure 4.

Each data point in Figure 4 is an average of five measurements independently made with five different transistors and the error bars are one standard deviation. These results compare favorably to the recently reported device (Xu *et al.*[51] in Table 1), which exhibited the same linear dynamic range: four decades of DNA concentration. In the studies summarized in Table 1, lowering the LoD had been attributed primarily to the material of the FET channel, e.g., moving from few-layer graphene to SLG[21] or from transferred to directly-grown CVD graphene.[51] The practical difficulties of reaching LoD < 1 nM have been noted in previous experimental[25] and theoretical[52] studies, as longer measurement times are required for a sufficient number of DNA targets to reach the sensor surface. The rationale for our optimization strategy was to increase the probability that the rare target arrival events to the sensor surface will encounter a probe and become successfully captured, via increasing the surface density of the probes and the ionic strength of the hybridization solution, given the well-known importance of these parameters.[36,37,40,43] The LoD achieved in our work clearly indicates that using transferred CVD-graphene as the channel material does not intrinsically limit the sensitivity of bio-FETs. Of course, in practical devices lowering the LoD results in shifting the dynamic range to lower DNA concentrations, e.g., the entire dynamic range demonstrated for the device in Ref [51] is within the saturation range of ours (Figure 4). Accordingly, bio-FET device optimization needs to be application-specific, to appropriately inform the choices of the design parameters.[36,37]

CONCLUSIONS

A bio-FET based on transferred CVD-graphene was successfully developed for the detection of DNA hybridization. The probe DNA molecules were immobilized on the graphene surface via NHS reaction with PBSE, a heterobifunctional linker. The unreacted NHS ligands of PBSE are then blocked by incubation with ethanolamine, to reduce nonspecific interactions during the subsequent measurements. The results show that the graphene bio-FET can detect target DNA molecules down to attomolar levels with a sensitivity of 24 mV/decade, with a dynamic range of 10^4.

This label-free graphene bio-FET has great potential, particularly for applications where the levels of mutated DNA are much higher than those of normal DNA, due to the ability to detect full hybridization down to 25 aM, compared to 5 orders of magnitude higher levels of SNP-containing targets. Further studies need to be performed in order to evaluate the performance of the bio-FET in the presence of interferents and complex matrices.

ASSOCIATED CONTENT

Supporting Information. Schematic representation of biosensor development, complete TC sets for all the stages and different concentrations, Raman spectra of the various stages,

XPS results, SEM images of the FET, non-normalized calibration curves, and electrochemical measurements including the experimental details.

AUTHOR INFORMATION

Corresponding Author

* pedro.alpuim.us@inl.int

Present Address

ζAXES Research Group, Chemistry Department, Groenenborgerlaan 171, 2020 Antwerp, Belgium

Author Contributions

Experiments were designed by R.C., J.B., and P.A. Fabrication of EGFETs and testing was performed by G.M.Jr., J.B. and R.C., graphene growth and transfer was performed by G.M.Jr., graphene characterization was performed by M.F.C, XPS and QCM measurements were performed by J.R.G. and D.Y.P. The manuscript and figures were prepared by R.C., J.B., M.F.C., J.R.G., D.Y.P, and P.A., P.A. supervised all aspects of this work. The manuscript was written through contributions of all authors. All authors have given approval to the final version of the manuscript.

Notes

The authors declare no competing financial interest.

ACKNOWLEDGMENT

This work was partially supported by the Portuguese Foundation for Science and Technology (FCT) in the framework of the Strategic Funding UID/FIS/04650/2013 and project POCI-01-0145-FEDER-031069 (PORTGRAPHE). G. Machado Jr. acknowledges a PhD grant (no. 237630/2012–5) from CNPq–Brazil. J.B. acknowledges European funding from NBFS project under contract NORTE-01-0145-FEDER-000019.

REFERENCES

(1) Janasek, D.; Franzke, J.; Manz, A. Scaling and the Design of Miniaturized Chemical-Analysis Systems. *Nature* **2006**, *442* (7101), 374–380.

(2) Barany, F. Genetic Disease Detection and DNA Amplification Using Cloned Thermostable Ligase. *Proc. Natl. Acad. Sci. U. S. A.* **1991**, *88* (1), 189–193. https://doi.org/10.1073/pnas.88.1.189.

(3) Shapiro, J. a. Genome Informatics: The Role of DNA in Cellular Computations. *Biol. Theory* **2006**, *1* (3), 288–301. https://doi.org/10.1162/biot.2006.1.3.288.

(4) Jin, L.; Chakraborty, R. Population Structure, Stepwise Mutations, Heterozygote Deficiency and Their Implications in DNA Forensics. *Heredity (Edinb).* **1995**, *74 (Pt 3)* (May 1994), 274–285. https://doi.org/10.1038/hdy.1995.41.

(5) Du, Y.; Guo, S.; Dong, S.; Wang, E. An Integrated Sensing System for Detection of DNA Using New Parallel-Motif DNA Triplex System and Graphene-Mesoporous Silica-Gold Nanoparticle Hybrids. *Biomaterials* **2011**, *32* (33), 8584–8592. https://doi.org/10.1016/j.biomaterials.2011.07.091.

(6) Mullis, K.; Faloona, F.; Scharf, S.; Saiki, R.; Horn, G.; Erlich, H. Specific Enzymatic Amplification of DNA in Vitro: The Polymerase Chain Reaction. *Cold Spring Harb. Symp. Quant Biol* **1986**, *51*, 263–273.

(7) Aleksić, M. M.; Kapetanović, V. An Overview of the Optical and Electrochemical Methods for Detection of DNA - Drug Interactions. *Acta Chimica Slovenica*. 2014, pp 555–573.

(8) Drummond, T. G.; Hill, M. G.; Barton, J. K. Electrochemical DNA Sensors. *Nat. Biotechnol.* **2003**, *21* (10), 1192–1199. https://doi.org/10.1038/nbt873.

(9) Park, H.-Y.; Dugasani, S. R.; Kang, D.-H.; Yoo, G.; Kim, J.; Gnapareddy, B.; Jeon, J.; Kim, M.; Song, Y. J.; Lee, S.; et al. M-DNA/Transition Metal Dichalcogenide Hybrid Structure-Based Bio-FET Sensor with Ultra-High Sensitivity. *Sci. Rep.* **2016**, *6* (October), 35733. https://doi.org/10.1038/srep35733.

(10) Sze, S. M.; Ng, K. K. Physics and Properties of Semiconductors—A Review. In *Physics of Semiconductor Devices*; John Wiley & Sons, Inc., 2006; pp 5–75. https://doi.org/10.1002/9780470068328.ch1.

(11) Veigas, B.; Fortunato, E.; Baptista, P. Field Effect Sensors for Nucleic Acid Detection: Recent Advances and Future Perspectives. *Sensors* **2015**, *15* (5), 10380–10398. https://doi.org/10.3390/s150510380.

(12) Justino, C. I. L.; Gomes, A. R.; Freitas, A. C.; Duarte, A. C.; Rocha-Santos, T. A. P. Graphene Based Sensors and Biosensors. *TrAC Trends Anal. Chem.* **2017**, *91*, 53–66. https://doi.org/10.1016/J.TRAC.2017.04.003.

(13) Bockris, J. O.; Devanathan, M. A. V.; Muller, K. On the Structure of Charged Interfaces. *Proc. R. Soc. A Math. Phys. Eng. Sci.* **1963**, *274* (1356), 55–79. https://doi.org/10.1098/rspa.1963.0114.

(14) Cui, Y.; Wei, Q.; Park, H.; Lieber, C. M. Nanowire Nanosensors for Highly Sensitive and Selective Detection of Biological and Chemical Species. *Science* **2001**, *293* (5533), 1289–1292. https://doi.org/10.1126/science.1062711.

(15) Yang, W.; Ratinac, K. R.; Ringer, S. R.; Thordarson, P.; Gooding, J. J.; Braet, F. Carbon Nanomaterials in Biosensors: Should You Use Nanotubes or Graphene. *Angewandte Chemie - International Edition*. 2010, pp 2114–2138. https://doi.org/10.1002/anie.200903463.

(16) Lee, J.; Dak, P.; Lee, Y.; Park, H.; Choi, W.; Alam, M. A.; Kim, S. Two-Dimensional Layered MoS_2 Biosensors Enable Highly Sensitive Detection of Biomolecules. *Sci. Rep.* **2014**, *4*, 7352. https://doi.org/10.1038/srep07352.

(17) Ohno, Y.; Maehashi, K.; Yamashiro, Y.; Matsumoto, K. Electrolyte-Gated Graphene Field-Effect Transistors for Detecting Ph and Protein Adsorption. *Nano Lett.* **2009**, *9* (9), 3318–3322. https://doi.org/10.1021/nl901596m.

(18) Ohno, Y.; Maehashi, K.; Matsumoto, K. Label-Free Biosensors Based on Aptamer-Modified Graphene Field-Effect Transistors. *J. Am. Chem. Soc.* **2010**, *132* (51), 18012–18013. https://doi.org/10.1021/ja108127r.

(19) Lee, D.-W.; Lee, J.; Sohn, I. Y.; Kim, B.-Y.; Son, Y. M.; Bark, H.; Jung, J.; Choi, M.; Kim, T. H.; Lee, C.; et al. Field-Effect Transistor with a Chemically Synthesized MoS2 Sensing Channel for Label-Free and Highly Sensitive Electrical Detection of DNA Hybridization. *Nano Res.* **2015**, *8* (7), 2340–2350. https://doi.org/10.1007/s12274-015-0744-8.

(20) Dong, X.; Shi, Y.; Huang, W.; Chen, P.; Li, L.-J. Electrical Detection of DNA Hybridization with Single-Base Specificity Using Transistors Based on CVD-Grown Graphene Sheets. *Adv. Mater.* **2010**, *22* (14), 1649–1653. https://doi.org/10.1002/adma.200903645.

(21) Chen, T.-Y.; Loan, P. T. K.; Hsu, C.-L.; Lee, Y.-H.; Tse-Wei Wang, J.; Wei, K.-H.; Lin, C.-T.; Li, L.-J. Label-Free Detection of DNA Hybridization Using Transistors Based on CVD Grown Graphene. *Biosens. Bioelectron.* **2013**, *41*, 103–109. https://doi.org/http://dx.doi.org/10.1016/j.bios.2012.07.059.

(22) Lin, C.-T.; Loan, P. T. K.; Chen, T.-Y.; Liu, K.-K.; Chen, C.-H.; Wei, K.-H.; Li, L.-J. Label-Free Electrical Detection of DNA Hybridization on Graphene Using Hall Effect Measurements: Revisiting the Sensing Mechanism. *Adv. Funct. Mater.* **2013**, *23* (18), 2301–2307. https://doi.org/10.1002/adfm.201202672.

(23) Zheng, C.; Huang, L.; Zhang, H.; Sun, Z.; Zhang, Z.; Zhang, G.-J. Fabrication of Ultrasensitive Field-Effect Transistor DNA Biosensors by a Directional Transfer Technique Based

on CVD-Grown Graphene. *ACS Appl. Mater. Interfaces* **2015**, *7* (31), 16953–16959. https://doi.org/10.1021/acsami.5b03941.

(24) Cai, B.; Wang, S.; Huang, L.; Ning, Y.; Zhang, Z.; Zhang, G.-J. Ultrasensitive Label-Free Detection of PNA–DNA Hybridization by Reduced Graphene Oxide Field-Effect Transistor Biosensor. *ACS Nano* **2014**, *8* (3), 2632–2638. https://doi.org/10.1021/nn4063424.

(25) Xu, S.; Zhan, J.; Man, B.; Jiang, S.; Yue, W.; Gao, S.; Guo, C.; Liu, H.; Li, Z.; Wang, J.; et al. Real-Time Reliable Determination of Binding Kinetics of DNA Hybridization Using a Multi-Channel Graphene Biosensor. *Nat. Commun.* **2017**, *8*, 14902. https://doi.org/10.1038/ncomms14902.

(26) Ohno, Y.; Okamoto, S.; Maehashi, K.; Matsumoto, K. Direct Electrical Detection of DNA Hybridization Based on Electrolyte-Gated Graphene Field-Effect Transistor. *Jpn. J. Appl. Phys.* **2013**, 52, 110107. https://doi.org/10.7567/JJAP.52.110107.

(27) Xu, G.; Abbott, J.; Qin, L.; Yeung, K. Y. M.; Song, Y.; Yoon, H.; Kong, J.; Ham, D. Electrophoretic and Field-Effect Graphene for All-Electrical DNA Array Technology. *Nat. Commun.* **2014**, 5, 4866. https://doi.org/10.1038/ncomms5866.

(28) Hybridization of two different strands of DNA or RNA | mfold.rit.albany.edu http://unafold.rna.albany.edu/?q=DINAMelt/Hybrid2.

(29) Campos, R.; Machado, G.; Cerqueira, M. F.; Borme, J.; Alpuim, P. Wafer Scale Fabrication of Graphene Microelectrode Arrays for the Detection of DNA Hybridization. *Microelectron. Eng.* **2018**, *189*, 85–90. https://doi.org/10.1016/J.MEE.2017.12.015.

(30) Vieira, N. C. S.; Borme, J.; Machado, G.; Cerqueira, F.; Freitas, P. P.; Zucolotto, V.; Peres, N. M. R.; Alpuim, P. Graphene Field-Effect Transistor Array with Integrated Electrolytic Gates Scaled to 200 Mm. *J. Phys. Condens. Matter* **2016**, *28* (8), 085302. https://doi.org/10.1088/0953-8984/28/8/085302.

(31) Aguiar, F. A.; Campos, R.; Wang, C.; Jitchati, R.; Batsanov, A. S.; Bryce, M. R.; Kataky, R. Comparative Electrochemical and Impedance Studies of Self-Assembled Rigid-Rod Molecular Wires and Alkanethiols on Gold Substrates. *Phys. Chem. Chem. Phys.* **2010**, *12* (44), 14804–14811. https://doi.org/10.1039/c005402j.

(32) Chen, R. J.; Zhang, Y.; Wang, D.; Dai, H. Noncovalent Sidewall Functionalization of Single-Walled Carbon Nanotubes for Protein Immobilization. *J. Am. Chem. Soc.* **2001**, *123* (16), 3838–3839. https://doi.org/10.1021/ja010172b.

(33) Tlili, C.; Cella, L. N.; Myung, N. V; Shetty, V.; Mulchandani, A. Single-Walled Carbon Nanotube Chemoresistive Label-Free Immunosensor for Salivary Stress Biomarkers. *Analyst* **2010**, *135* (10), 2637–2642. https://doi.org/10.1039/c0an00332h.

(34) Mayorov, A. S.; Elias, D. C.; Mukhin, I. S.; Morozov, S. V.; Ponomarenko, L. A.; Novoselov, K. S.; Geim, A. K.; Gorbachev, R. V. How Close Can One Approach the Dirac Point in Graphene Experimentally? *Nano Lett.* **2012**, *12* (9), 4629–4634. https://doi.org/10.1021/nl3019222d.

(35) Chen, J.-H.; Ishigami, M.; Jang, C.; Hines, D. R.; Fuhrer, M. S.; Williams, E. D. Printed Graphene Circuits. *Adv. Mater.* **2007**, *19* (21), 3623–3627. https://doi.org/10.1002/adma.200701059.

(36) Gong, P.; Chi-Ying Lee; Lara J. Gamble; Castner, D. G.; David W. Grainger. Hybridization Behavior of Mixed DNA/Alkylthiol Monolayers on Gold: Characterization by Surface Plasmon Resonance and 32P Radiometric Assay. **2006**. https://doi.org/10.1021/AC052138B.

(37) Schreiner, S. M.; Shudy, D. F.; Hatch, A. L.; Opdahl, A.; Whitman, L. J.; Petrovykh, D. Y. Controlled and Efficient Hybridization Achieved with DNA Probes Immobilized Solely through Preferential DNA-Substrate Interactions. *Anal. Chem.* **2010**, *82* (7), 2803–2810. https://doi.org/10.1021/ac902765g.

(38) Alloway, D. M.; Hofmann, M.; Smith, D. L.; Gruhn, N. E.; Graham, A. L.; Colorado, R.; Wysocki, V. H.; Lee, T. R.; Lee, P. a; Armstrong, N. R. Interface Dipoles Arising from Self-Assembled Monolayers on Gold: UV-Photoemission Studies of Alkanethiols and Partially Fluorinated Alkanethiols. *J. Phys. Chem. B* **2003**, *107* (42), 11690–11699. https://doi.org/10.1021/jp034665+.

(39) Lerner, M. B.; Resczenski, J. M.; Amin, A.; Johnson, R. R.; Goldsmith, J. I.; Johnson, A. T. C. Toward Quantifying the Electrostatic Transduction Mechanism in Carbon Nanotube Molecular Sensors. *J. Am. Chem. Soc.* **2012**, *134* (35), 14318–14321. https://doi.org/10.1021/ja306363v.

(40) Campos, R.; Ferapontova, E. E. Electrochemistry of Weakly Adsorbed Species: Voltammetric Analysis of Electron Transfer between Gold Electrodes and Ru Hexaamine Electrostatically Interacting with DNA Duplexes. *Electrochim. Acta* **2014**, *126*, 151–157. https://doi.org/10.1016/j.electacta.2013.07.083.

(41) Álvarez-Martos, I.; Campos, R.; Ferapontova, E. E. Surface State of the Dopamine RNA Aptamer Affects Specific Recognition and Binding of Dopamine by the Aptamer-Modified Electrodes. *Analyst* **2015**, *140* (12), 4089–4096. https://doi.org/10.1039/c5an00480b.

(42) Ray, S.; Steven, R. T.; Green, F. M.; Höök, F.; Taskinen, B.; Hytönen, V. P.; Shard, A. G. Neutralized Chimeric Avidin Binding at a Reference Biosensor Surface. *Langmuir* **2015**, *31* (6), 1921–1930. https://doi.org/10.1021/la503213f.

(43) Petrovykh, D. Y.; Kimura-Suda, H.; Tarlov, M. J.; Whitman, L. J. Quantitative Characterization of DNA Films by X-Ray Photoelectron Spectroscopy. *Langmuir* **2004**, *20* (2), 429–440. https://doi.org/10.1021/LA034944O.

(44) Petrovykh, D. Y.; Kimura-Suda, H.; Opdahl, A.; Richter, L. J.; Tarlov, M. J.; Whitman, L. J. Alkanethiols on Platinum: Multicomponent Self-Assembled Monolayers. *Langmuir* **2006**, *22* (6), 2578–2587. https://doi.org/10.1021/LA050928A.

(45) Fears, K. P.; Clark, T. D.; Petrovykh, D. Y. Residue-Dependent Adsorption of Model Oligopeptides on Gold. *J. Am. Chem. Soc.* **2013**, *135* (40), 15040–15052. https://doi.org/10.1021/ja4043469p.

(46) Lim, C. Y.; Owens, N. A.; Wampler, R. D.; Ying, Y.; Granger, J. H.; Porter, M. D.; Takahashi, M.; Shimazu, K. Succinimidyl Ester Surface Chemistry: Implications of the Competition between Aminolysis and Hydrolysis on Covalent Protein Immobilization. *Langmuir* **2014**, *30* (43), 12868–12878. https://doi.org/10.1021/la5034399g.

(47) Sherbet, G. V; Lakshmi, M. S.; Cajone, F. Isoelectric Characteristics and the Secondary Structure of Some Nucleic Acids. *Biophys. Struct. Mech.* **1983**, *10* (3), 121–128. https://doi.org/10.1007/BF00537554.

(48) Yin, Z.; He, Q.; Huang, X.; Zhang, J.; Wu, S.; Chen, P.; Lu, G.; Chen, P.; Zhang, Q.; Yan, Q.; et al. Real-Time DNA Detection Using Pt Nanoparticle-Decorated Reduced Graphene Oxide Field-Effect Transistors. *Nanoscale* **2012**, *4* (1), 293–297. https://doi.org/10.1039/C1NR11149C.

(49) Dong, X.; Fu, D.; Fang, W.; Shi, Y.; Chen, P.; Li, L.-J. Doping Single-Layer Graphene with Aromatic Molecules. *Small* **2009**, 5 (12), 1422–1426. https://doi.org/10.1002/smll.200801711.

(50) Zhang, Z.; Huang, H.; Yang, X.; Zang, L. Tailoring Electronic Properties of Graphene by Π–π Stacking with Aromatic Molecules. *J. Phys. Chem. Lett.* **2011**, *2* (22), 2897–2905. https://doi.org/10.1021/jz201273r.

(51) Xu, S.; Jiang, S.; Zhang, C.; Yue, W.; Zou, Y.; Wang, G.; Liu, H.; Zhang, X.; Li, M.; Zhu, Z.; et al. Ultrasensitive Label-Free Detection of DNA Hybridization by Sapphire-Based Graphene Field-Effect Transistor Biosensor. *Appl. Surf. Sci.* **2018**, *427*, 1114–1119.

https://doi.org/10.1016/j.apsusc.2017.09.113.

(52) Sheehan, P. E.; Whitman, L. J. Detection Limits for Nanoscale Biosensors. *Nano Lett.* **2005**. https://doi.org/10.1021/nl050298x.

For TOC only